JOURNAL OF MATERIALS SCIENCE 29 (1994) 2119–2125

Microwave and conventional sintering of rapidly solidified Al_2O_3–ZrO_2 powders

J. McKITTRICK, B. TUNABOYLU
Materials Science Program, University of California, San Diego, La Jolla, CA 92093-0411, USA

J. KATZ
Los Alamos National Laboratory, Mail Stop G771, Los Alamos, NM 87545, USA

The Al_2O_3–ZrO_2 eutectic composition was rapidly solidified, forming amorphous and crystalline structures. The as-quenched material was crushed and pressed into pellets which were sintered conventionally or with microwaves. Conventional and microwave sintering at temperatures up to 1600 °C resulted in a microstructure where 100–200 nm ZrO_2 grains were present intergranularly in the α-Al_2O_3 grains. Larger ZrO_2 grains ($\sim$1 μm) were found intergranularly. The as-quenched lamellar structure spheroidized during sintering at high temperatures. Boron contamination of the powders resulted in more homogeneous and dense as-fired samples but promoted the ZrO_2 tetragonal-to-monoclinic transformation, which was attributed to increased grain boundary diffusivity. Conventional sintering at low temperatures resulted in the formation of "rods" of an Al_2O_3-rich phase which grew from a low-melting B_2O_3-rich liquid.

1. Introduction

Rapid solidification processing (RSP) is a technique used to generate materials with unusual microstructures and properties which cannot be obtained through other synthesis methods. Most of the work in this area has been on metallic systems since Duwez *et al.* [1] discovered in 1960 that splatting a liquid metal against a cold substrate resulted in the formation of a metallic glass. Sarjeant and Roy [2] first applied this technique to various oxides in 1967. Quench rates reported for rapid solidification of oxides range from 10^3 to 10^9 K s^{-1} [3, 4].

Rapid solidification rates suppress diffusion in both the liquid and solid and hence curb the formation of the equilibrium phases and microstructures found in slowly cooled materials. Materials produced through rapid solidification have several advantages. First, increasing the solidification rate results in a smaller size. Second, the grains are chemically homogeneous and have limited or no grain boundary segregation of impurities. Third, faster quench rates can extend the terminal solid solubility of the primary phase. Finally, metastable phases can be quenched-in from a melt, including supersaturated or amorphous materials.

The fine-grained or amorphous structure of rapidly solidified materials will not necessarily be retained after densification, which typically involves sintering at high temperatures. Microwave sintering is a technique in which the samples are heated rapidly to high temperatures to promote densification and reduce grain growth [5, 6]. We examined the compaction behaviour and microstructural features of conventionally sintered and microwave-sintered rapidly solidified powders of the eutectic composition in the Al_2O_3–ZrO_2 system.

2. Experimental procedure

Technical-grade commercial powders of 61.9 mol % (57.4 wt %) α-Al_2O_3 and 32.1 mol % (42.6 wt %) monoclinic ZrO_2 (m-ZrO_2) were mixed and pressed to form rods of $\sim$ 6 cm length and 1 cm diameter. The rods were suspended above a twin-roller solidification device and were heated with an oxyhydrogen torch. Liquid droplets formed on the end of the rod and were allowed to drop between the rollers, rotating with surface speeds of $\sim$ 10 m s^{-1} Fig. 1 shows a schematic diagram of the rapid solidification device.

The as-quenched materials were ball-milled in ethanol overnight with Al_2O_3 or B_4C media, dried and then sieved through 45 μm. The resultant starting powder was composed of angular and sharp particles with a large size distribution. The materials milled in B_4C transformed from a white powder to a light grey colour. The powders were cold-pressed at 350 MPa into 1.27 cm diameter, 4 mm thick discs and then sintered for 2 h at 1200, 1400 and 1600 °C. The heating rate was $\sim$ 10 °C min^{-1}.

Other samples were microwave-sintered at 1400, 1600 or 1650 °C. The average ramp time to the high temperature was 10–15 min. The samples were not held at T_{max}. The microwave furnace consists of a 2.45 GHz, 6 kW generator and a 2 ft^3 (5.7×10^{-2} m^2) resonant cavity. Temperature was measured with a multichannel optical fibre thermometer. The compacted samples were examined by X-ray diffraction

0022–2461

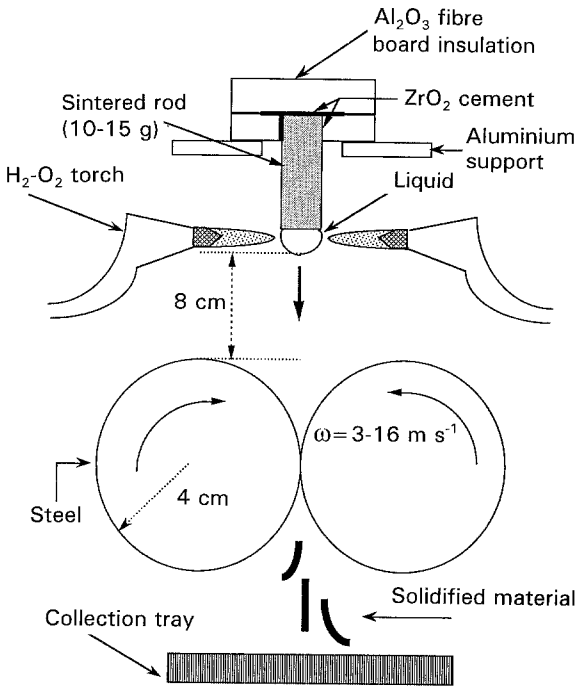

Figure 1 Schematic diagram of rapid solidification device.

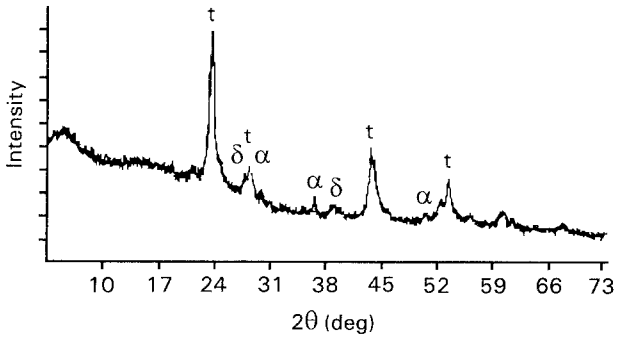

Figure 2 X-ray diffraction pattern of as-quenched material. Peaks correspond to α + δ-Al_2O_3 and tetragonal ZrO_2.

and SEM. Bulk density was measured using the Archimedes principle.

3. Results and discussion

3.1. As-quenched materials

The as-quenched samples are nanocrystalline or submicrocrystalline, as seen in the X-ray diffraction trace of Fig. 2. The peaks index to tetragonal ZrO_2 (t-ZrO_2) and a mixture of (δ + α)-Al_2O_3. Amorphous material is also present as seen by the large, amorphous hump present in the low-angle region. This is in agreement with other results found for these materials [7–9]. The TEM micrographs in Fig. 3 show several of the microstructures observed in the as-quenched materials in different regions of the sample. A nanocrystalline and amorphous structure is shown in Fig. 3a and b. A eutectic solidification microstructure with lamellae of both Al_2O_3 and ZrO_2 is present in Fig. 3c. The microstructural variety is a result of differing local solidification conditions, which arise due to the rollers progressively becoming scratched and gouged during repeated runs.

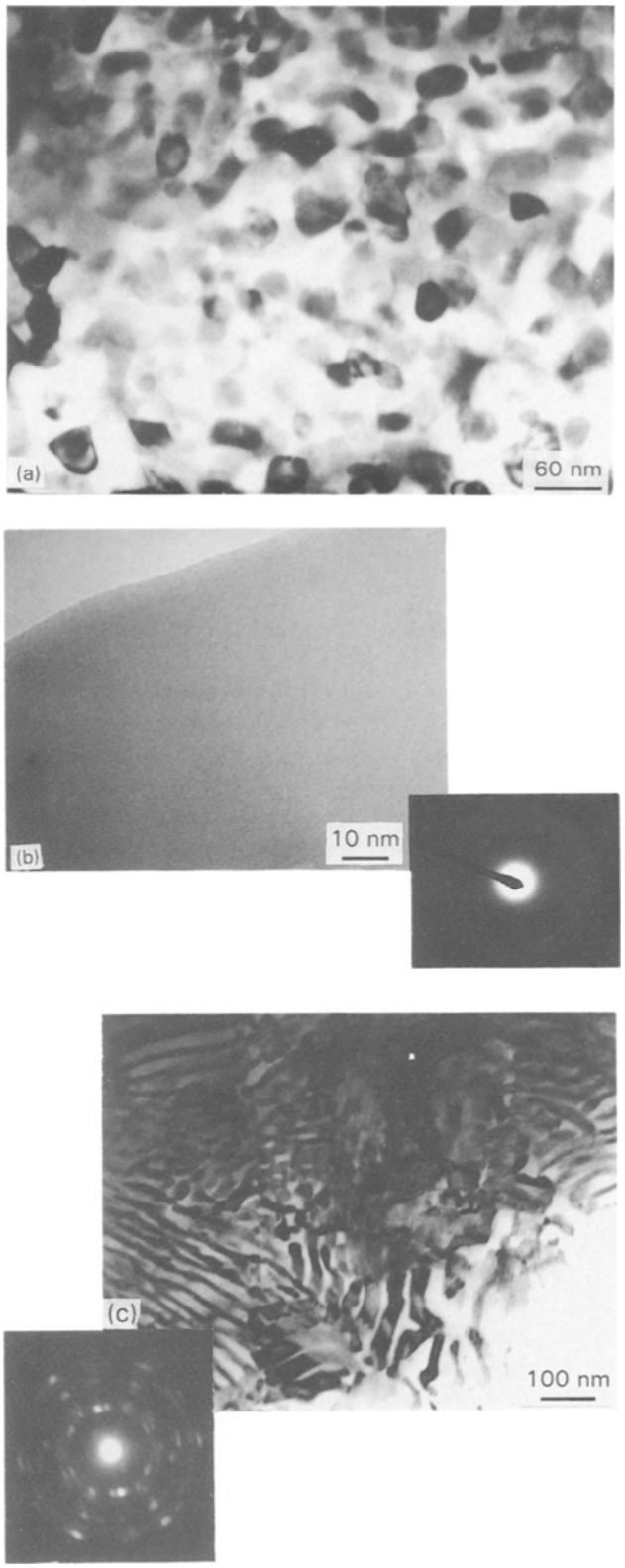

Figure 3 TEM micrographs of the as-quenched material: (a) nanocrystalline region, (b) amorphous region, (c) fine lamellar eutectic microstructure.

3.2. Conventional sintering

Microstructural differences between materials milled with Al_2O_3 and B_4C during conventional sintering are seen in Fig. 4a and b respectively. Both materials were heated to 1200 °C for 2 h. The material milled in Al_2O_3 shows no features and the coarse and angular nature of the starting material is clearly seen. No sintering has occurred. The phase assemblage consists

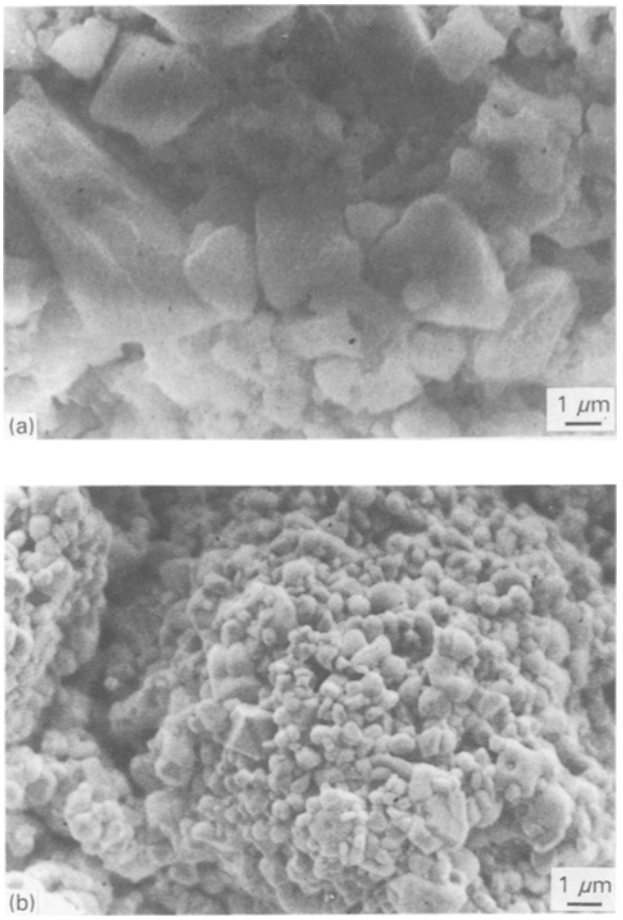

Figure 4 SEM of conventional sintering at 1200 °C for 2 h for material milled in (a) Al_2O_3, (b) B_4C.

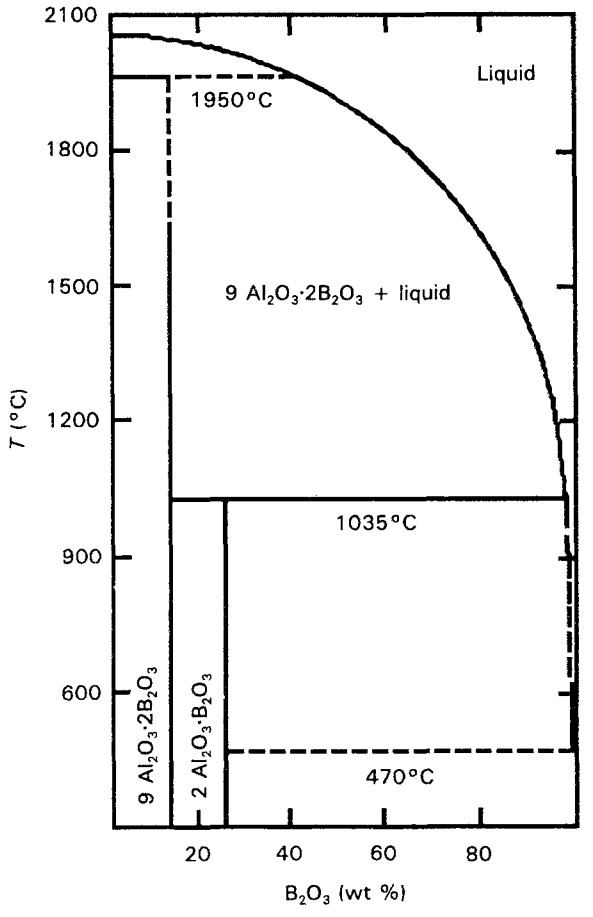

Figure 5 Al_2O_3–B_2O_3 phase diagram [10].

of t-ZrO_2 and α-Al_2O_3. All of the δ-Al_2O_3 in the as-quenched material has transformed into the α-phase. For the material milled in B_4C, small nucleation events are observed in the starting material. Small nuclei which range from 200–800 nm occur homogeneously on the surface. This can be attributed to the B_4C contamination in the powder which has oxidized to form B_2O_3 and CO_2 at high temperatures. Fig. 5 shows the phase diagram for Al_2O_3–B_2O_3 [10]. At 1200 °C a liquid phase is present for compositions of > 18 mol % B_2O_3, yielding equilibrium between the $9Al_2O_3{\cdot}2B_2O_3$ solid phase and a B_2O_3-rich liquid phase. Cooling from this two-phase region would yield a two-phase solid mixture of $9Al_2O_3{\cdot}2B_2O_3$ and $2Al_2O_3{\cdot}B_2O_3$ for compositions between 18.2 and 33.3 mol % B_2O_3. Both phases are orthorhombic and have *d* spacings which are indistinguishable from each other in our X-ray patterns due to the low concentrations.

Further evidence for the presence of a liquid phase is shown in the material heated to 1400 °C shown in Fig. 6a. "Rods" of an Al_2O_3-rich phase, whose composition was determined by energy-dispersive spectroscopy in the SEM, are dispersed with small, round grains of ZrO_2. The rods are several micrometres long and about 200 nm in diameter. Rod-type growth is often found in systems in which a small amount of liquid is present. At 1600 °C the microstructure consists of small ZrO_2 grains (light phase) ranging from

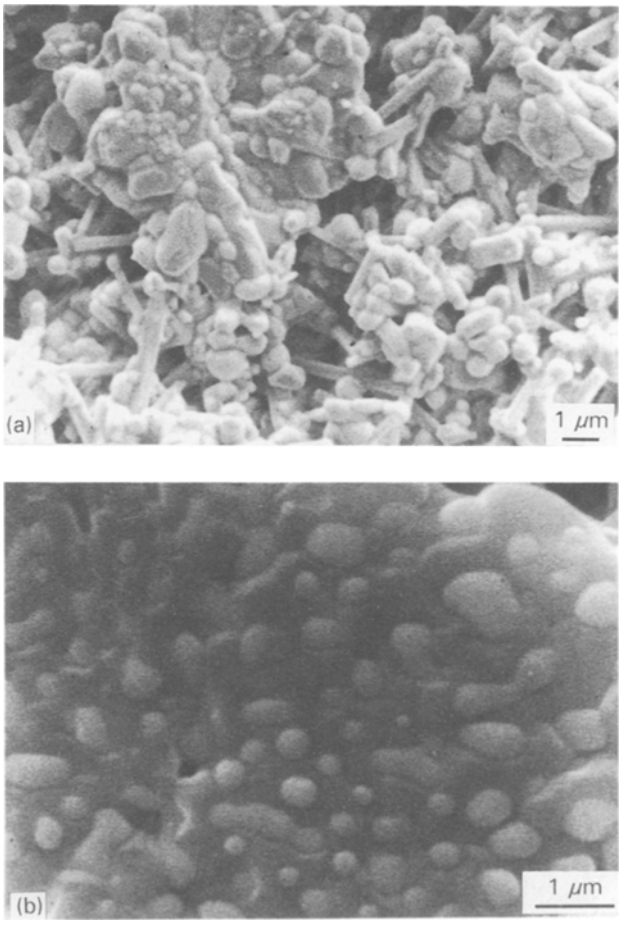

Figure 6 SEM of material milled in B_4C and conventionally sintered for 2 h at (a) 1400 °C, (b) 1600 °C.

TABLE I Bulk densities of conventional and microwave-sintered materials

Temperature (°C)	Milling medium	Time (h)	Density ($g\,cm^{-3}$)
Conventional			
1200	Al_2O_3	2	82.0
	B_4C	2	70.0
1400	Al_2O_3	2	88.0
	B_4C		74.0
1600	B_4C	2	95.3
Microwave			
1400	Al_2O_3	–[a]	69.5
	B_4C	–[a]	78.5
1600	Al_2O_3	–[a]	88.4
	B_4C	–[a]	
1650	Al_2O_3	–[a]	88.4
	B_4C	–[a]	78.2

[a]Not held at T_{max}.

200 nm to 1 μm in diameter dispersed in the Al_2O_3 matrix (dark phase), as shown in Fig. 6b.

The densities of the sintered samples are listed in Table I. Higher sintering temperatures and the presence of boron increase the bulk densities. We have achieved densities as high as 95% of ρth for conventional sintering at 1600 °C. Small additions of boron to Al_2O_3 have been found to significantly increase the density of sintered Al_2O_3 [11]. X-ray diffraction results show that the retention of t-ZrO_2 is significantly influenced by the presence of boron in the sample, as listed in Table II. The amount of t-ZrO_2 is found from [12]

$$f_t = \frac{I_t(1\,1\,1)}{I_t(1\,1\,1) + I_m(1\,1\,1) + I_m(1\,1\,\bar{1})} \quad (1)$$

where $I_t(1\,1\,1)$ is the intensity of the (1 1 1) t-ZrO_2 peak, $I_m(1\,1\,1)$ is that of the (1 1 1) m-ZrO_2 peak and I_m $(1\,1\,\bar{1})$ that of the $(1\,1\,\bar{1})$ peak of m-ZrO_2. At a temperature of 1200 °C, without boron the sample is 100% t-ZrO_2 while the boron-contaminated sample has only 44%. At progressively higher sintering temperatures, the fraction of retained t-ZrO_2 reduces further until only 17% is present after sintering at 1600 °C.

The higher fraction of m-ZrO_2 in the boron-contaminated samples can be explained by three factors: (i) the elastic modulus of the $Al_2O_3{\cdot}B_2O_3$ compound is thought not to be as high as for pure Al_2O_3, thereby reducing the elastic constraint of the matrix surrounding the ZrO_2 grains; (ii) the presence of boron in ZrO_2 promotes the t → m transformation; and/or (iii) the presence of the liquid phase enhances grain-boundary diffusivity and promotes grain growth. When t-ZrO_2 is heated grain growth is also accompanied by the t-m phase transformation at a critical grain size and temperature [13]. Factor (ii) seems unlikely as boron has limited solubility in ZrO_2. Buchanan and Wilson [14] have studied the effect of adding Al_2O_3 and B_2O_3 to yttria-stabilized ZrO_2 and found that significant densification resulted from liquid-phase sintering, but no transformation was observed in the ZrO_2 phase.

3.3. Microwave sintering

Interparticle sintering occurs during microwave sintering, as shown in Fig. 7a. The high degree of surface porosity can be attributed to the rather large and irregular starting material. Higher magnifications shown in Fig. 7b and c show 1–2 μm Al_2O_3 grains with intra- and intergranular ZrO_2 grains. The intragranular ZrO_2 has a very fine grain size, ranging from 100–200 nm, whereas the intragranular ZrO_2 is coarser, of the order of 0.5–1 μm. This larger Al_2O_3 grain size is a result of not adding a grain growth inhibitor to the starting material before solidification processing [15].

The intragranular ZrO_2 is thought to be a result of the solidification synthesis. It is well known that rapid solidification processing can produce supersaturation of one component in the other. High degrees of supersaturated ZrO_2 in the Al_2O_3 would precipitate in the grains at higher temperatures. These precipitates would be inhibited from growing further due to long-range diffusional problems as well as physical confinement in a well-crystallized region. Heuer *et al.* [16] have reported the synthesis of intragranular 8 vol % t-ZrO_2 in Al_2O_3 by hot-pressing sol–gel derived materials for 30 min at 1500 °C. The intragranular ZrO_2 averaged 0.5 μm and 85% of the Al_2O_3 grains were > 10 μm. In their study, rapid grain growth of the Al_2O_3 enveloped the ZrO_2 which prevented further growth. Virtually all of the ZrO_2 grains were intergranular at higher fractions of ZrO_2. Our materials

TABLE II X-ray diffraction results for conventional and microwave-sintered materials

Temperature (°C)	Medium	Phases present	Percentage tetragonal
Conventional			
1200	Al_2O_3	t-ZrO_2 + α-Al_2O_3	100
	B_4C	α-Al_2O_3,(t + m)ZrO_2, Al_2O_3-B_2O_3 phases*	44
1400	B_4C	α-Al_2O_3,(t + m)ZrO_2, Al_2O_3-B_2O_3 phases	31
1600	B_4C	α-Al_2O_3,(t + m)ZrO_2, Al_2O_3-B_2O_3 phases	17
Microwave			
1400	Al_2O_3	α-Al_2O_3,(t + m)ZrO_2	90
	B_4C	α-Al_2O_3,(t + m)ZrO_2, Al_2O_3-B_2O_3 phases	20
1600	Al_2O_3	α-Al_2O_3,(t + m)ZrO_2	31
1650	B_4C	α-Al_2O_3,(t + m)ZrO_2, Al_2O_3-B_2O_3 phases	17

* Combination of $9Al_2O_3{\cdot}2B_2O_3$ and $2Al_2O_3{\cdot}B_2O_3$

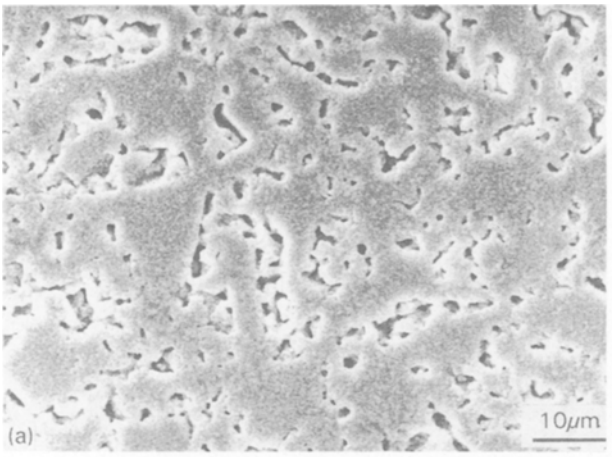

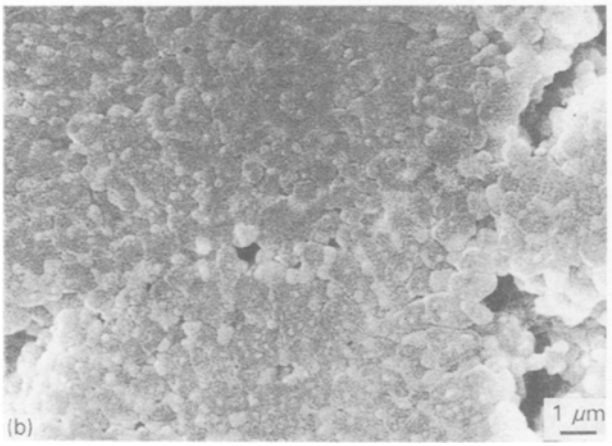

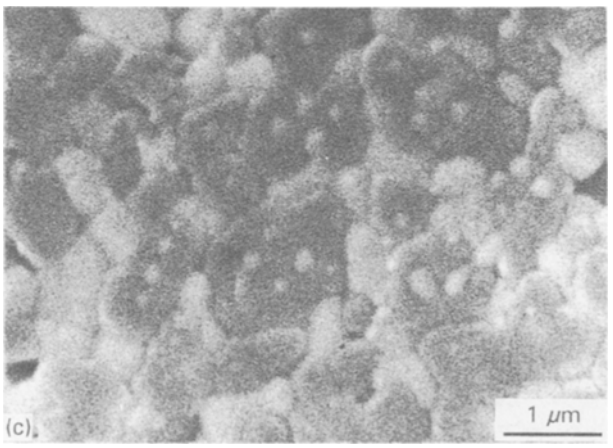

Figure 7 SEM micrographs of microwave sintering at 1600 °C showing (a) large voids, (b) interparticle sintering and (c) ZrO_2 grains in the Al_2O_3 matrix.

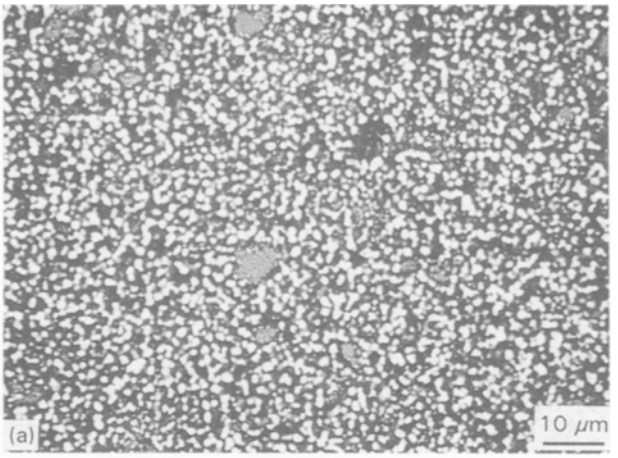

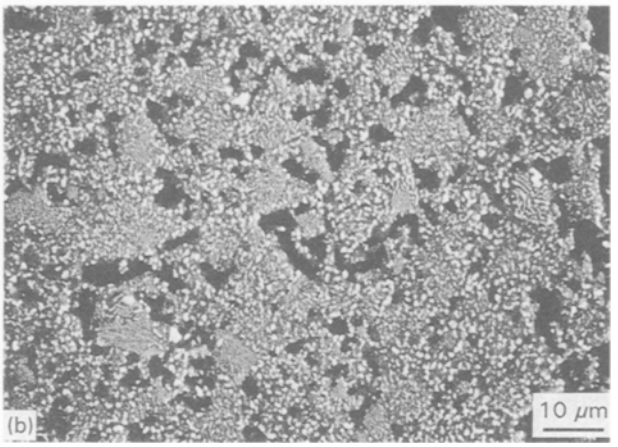

Figure 8 Backscattered SEM micrographs of microwave sintering for 10 min at 1650 °C for (a) boron-contaminated and (b) uncontaminated material.

have 38 vol % ZrO_2 and possess a high population of intragranular ZrO_2, suggesting that some arose from precipitation of supersaturated Al_2O_3 grains.

For microwave sintering at 1650 °C, the boron-contaminated sample shows a greatly reduced amount of surface porosity, as shown in the backscattered SEM micrograph in Fig. 8a. There are still some large pores, but the microstructure is remarkably homogeneous. The shapes of the irregular starting powders are not apparent, in contrast to the uncontaminated sample shown in Fig. 8b. In both cases, the Al_2O_3 and ZrO_2 are spherical but are larger for the boron contaminated sample. The 1400 °C sintered microstructure of the samples with and without the boron are shown Fig. 9a and b, respectively. The subgrain structure for both consists of regions of lamellar eutectic colonies. The rod-like structure of the Al_2O_3-B_2O_3 phase is not present in these microwave sintered materials, due to the inherent brief thermal cycle of microwave heating. The sample is not at a high enough temperature for the amount of time needed to grow Al_2O_3-B_2O_3 rods. In addition, there is no evidence for liquid phase sintering at this temperature as the surface porosities of samples with and without boron are similar.

The densities of the microwave-sintered samples do not display the same dramatic increase with temperature as do the conventionally sintered materials. The highest density was found for sintering at 1650 °C with the Al_2O_3 milling media at 88% of ρ_{th}. It appears that liquid-phase sintering is not achieved for the brief time–temperature cycle of this sintering technique.

The amount of t-ZrO_2 retained in the samples shows the same trend as with the conventionally sintered material, as shown by the X-ray data in Table II. At 1400 °C, there is 90% t-ZrO_2 which reduces to 17% at 1650 °C. Although the rod-like growth of Al_2O_3–B_2O_3 is not observed, the phase is present and significantly reduces the t-ZrO_2 content. Thus, growth of the ZrO_2 grains appears to be from higher grain-boundary diffusivities due to the presence of the Al_2O_3–B_2O_3 liquid (factor (iii) from above), and

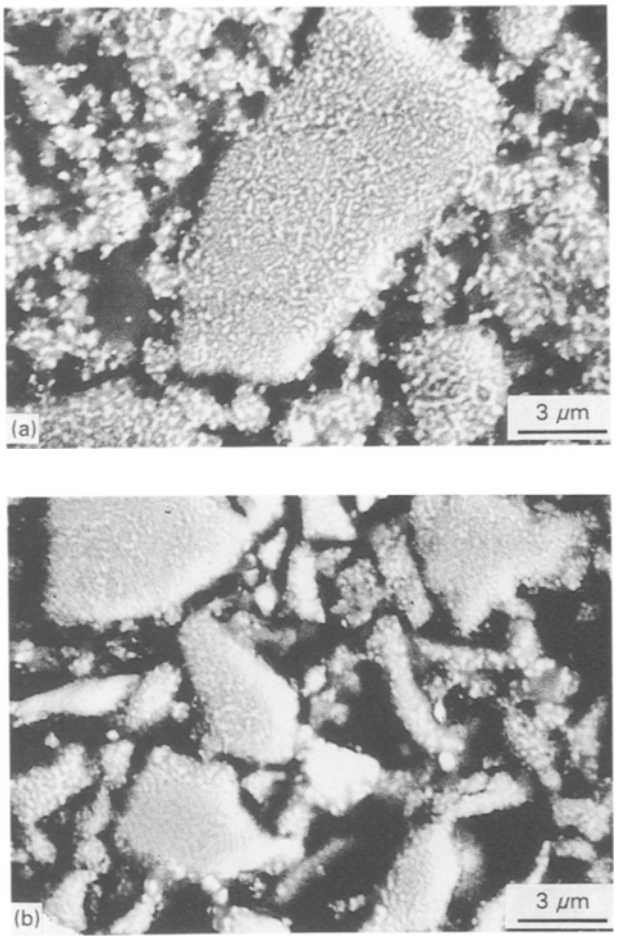

Figure 9 Backscattered SEM micrographs of microwave sintering for 10 min at 1400 °C for (a) boron-contaminated and (b) uncontaminated material.

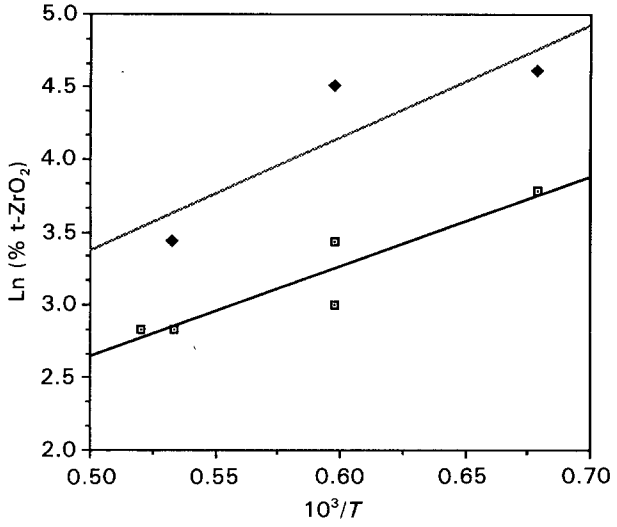

Figure 10 Amount of t-ZrO_2 in (⊡) B_4C (boron)-contaminated and (◆) uncontaminated (alumina) samples as a function of sintering temperature.

not the reduction of the elastic modulus of the surrounding material (factor (i) from above).

The amount of t-ZrO_2 retained in the samples conventionally sintered and microwave-sintered is plotted against reciprocal temperature, as shown in Fig. 10. A linear relationship is found which can be expressed for the Al_2O_3-milled materials as

$$\%\ \text{t-}ZrO_2 = 0.60 \exp\left(\frac{64.66\ \text{kJ mol}^{-1}}{RT}\right) \quad (2)$$

and for the boron-contaminated materials as

$$\%\ \text{t-}ZrO_2 = 0.66 \exp\left(\frac{50.08\ \text{kJ mol}^{-1}}{RT}\right) \quad (3)$$

The activation energies are low compared to activation energies for cation diffusion in ZrO_2, which are of the order of 100 kJ mol^{-1} [17]. These activation energies can be related to the grain-boundary diffusivities for growth of the ZrO_2 phase. As expected, the activation energy for the boron contaminated sample is lower than for the uncontaminated sample, which can be attributed to the presence of an Al_2O_3–B_2O_3 liquid.

4. Conclusions

The as-quenched microstructures of the eutectic composition in the Al_2O_3–ZrO_2 system are composed of amorphous and crystalline regions. Conventional sintering results in low densities of the pure material. Boron contamination, introduced from milling media, promotes nucleation and growth from the liquid phase of "rods" of a Al_2O_3–B_2O_3 phase from the liquid. Conventional sintering at high temperatures results in nanosize ZrO_2 grains embedded in the Al_2O_3 phase and high densities were achieved due to liquid-phase sintering. For microwave sintering, interparticle sintering is seen at 1600 °C and the microstructure is composed of nanocrystalline grains of ZrO_2 intragranularly present in micrometre-sized Al_2O_3 grains and micrometre and submicrometre grains of ZrO_2 intergranularly dispersed. Backscattered SEM images show the presence of lamellar eutectic colonies at 1400 °C which spheroidize at 1650 °C for both boron-contaminated and pure material. The activation energy for growth of the ZrO_2 phase was higher in the boron-contaminated then in the uncontaminated sample. This was attributed to a higher grain-boundary diffusivity due to the presence of an Al_2O_3–B_2O_3 liquid phase during sintering. The bulk densities for both sintering procedures have not been optimized. Obtaining a finer particle size distribution of the milled, as-quenched material will result in higher densities.

Acknowledgements

The authors gratefully acknowledge the Advanced Technology Assessment Center at the Los Alamos National Laboratory for supporting this work.

References

1. P. DUWEZ, R. H. WILLENS and W. KLEMENT, *J. Appl. Phys.* **31** (1960) 1136.
2. P. T. SARGEANT and R. ROY, *J. Amer. Ceram. Soc.* **50** (1967) 500.
3. M. C. BROCKWAY and R. R. WILLS, "Rapid Solidification of Ceramics – A Technology Assessment", Metals and Ceramics Information Center Report MCIC 84-49 (Battelle Columbus Laboratories, Columbus, Ohio, 1984).

4. A. REVCOLEVSCHI and J. LIVAGE, in "Treatise on Materials Science and Technology", Vol. 20, edited by H. Herman (Academic, New York, 1981) p. 73.
5. J. D. KATZ and R. D. BLAKE, *Ceram. Bull.* **70** (1991) 1304.
6. J. EASTMAN, K. SICKAFUS, J. KATZ, S. BOEKE, R. BLAKE, C. EVANS, R. SCHWARZ and Y. LIAO, *Mater. Res. Soc. Symp. Proc.* **189** (1991) 273.
7. J. McKITTRICK, G. KALONJI and T. ANDO, *J. Non-Cryst. Solids* **94** (1987) 163.
8. T. WHITNEY, V. JAYARAM, C. G. LEVI, and R. MEHRABIAN, in "Solidification Processing of Eutectic Alloys", edited by D. M. Stefanescu, G. J. Abbaschian and R. FJ. Bayuzick (Metallurgical Society, Warrendale, PA, 1988) p. 199.
9. N. CLAUSSEN, G. LINDEMANN and G. PETZOW, *Ceram. Int.* **9** (3) (1983) 83.
10. P. J. M. GIELISSE and W. R. FOSTER, *Nature* **195** (1962) 70.
11. L. A. XUE and I. W. CHEN, *J. Amer. Ceram. Soc.* **74** (1991) 2011.
12. R. C. GARVIE, R. H. J. HANNINK and M. V. SWAIN, *J. Mater. Sci. Lett.* **11** (1983) 437.
13. B. N. CLAUSSEN and M. RÜHLE, *Adv. Ceram.* **3** (1981) 137.
14. R. C. BUCHANAN and C. M. WILSON, *Gov. Rep. Announce. Index* **85** (8) (1985) 111.
15. M. P. HARMER, in "Structure and Properties of MgO and Al_2O_3 Ceramics", Advances in Ceramics, Vol. 10, edited by W. D. Kingery (American Ceramic Society, Columbus, OH, 1984) p. 679.
16. A. HEUER, N. CLAUSSEN, W. M. KRIVEN and M RÜHLE, *J. Amer. Ceram. Soc.* **65** (1982) 642.
17. J. BAUMARD and P. ABELARD, in "Advances in Ceramics", Vol. 12, edited by N. Claussen, M. Rühle and A. Heuer (American Ceramic Society, Columbus, Ohio, 1984) p. 555.

Received 12 January
and accepted 31 August 1993